An Extended List-Mode MLEM Algorithm for 3D Compton Image Reconstruction from Multi-View Data

Nhan Le[1,*], Hichem Snoussi[1], Zied Hmissi[2], Alain Iltis[2], Guillaume Lebonvallet[1], and Ghislain Zeufack[2]
[1]Computer Science and Digital Society laboratory, Troyes University of Technology, France
[2]Damavan Imaging, 2 rue Gustave Eiffel, 10430 Rosières-Près-Troyes, France
(*) thi-ai-nhan.le@utt.fr

***Abstract*—The lack of parallax in the measurements is a big challenge in 3D image reconstruction for handheld Compton cameras. Our solution to this issue is to extend the conventional list-mode maximum-likelihood expectation-maximization (LM-MLEM) 3D reconstruction algorithm to allow the simultaneous use of multi-view Compton data seeking parallax improvement. It involves building a new list-mode simultaneous data space from multi-view Compton events, formulating the associated probabilistic models for the system response matrix and sensitivity, and developing an extended LM-MLEM algorithm. For the performance assessment, we experiment the extended 3D reconstruction algorithm on real multi-view data conducted with a handheld CeBr3 Compton camera developed by Damavan Imaging and a punctual 0.2 (MBq) ^{22}Na source. Various comparative studies with different view numbers, source locations and energy ranges confirm the outperformances of our extended LM-MLEM algorithm.**

***Keywords* —3D reconstruction, handheld Compton camera, LM-MLEM algorithm, multi-view Compton events, real data.**

I. Introduction

3D Compton image reconstruction allows to visualize gamma ray sources in a given space by measuring a Compton scatter and a photoelectric absorption for each radioactive decay in terms of positions and deposited energies. This technique covers nowadays a wide range of applications in nuclear industry, medical imaging, homeland security and astronomy. In principle, the radioactive source related to a measured event is located on a cone surface issued from the Compton kinematics with the measured information. By drawing and overlaying multiple cones given from different measured events, we can retrieve the source location. Based on this idea, the literature has developed numerous reconstruction methods in two main streams: (*i*) *analytical inversion* [1] and (*ii*) *iterative model-based* [2]. The first stream exploits the relationship between a function and its line integrals. Although it often leads to fast reconstruction algorithms such as filtered back-projection [3], the accuracy of reconstructed images is limited, as it requires approximations in the line-integral model while eliminating uncertainties inherent in photon-limited detection. In contrast, the second stream enables more accurate reconstruction algorithms by explicitly modeling statistical variations in the photon detection process and progressively refining reconstructed images through repetitive calculations. The price of this accuracy is the significantly higher computational cost. This is why the current state-of-the-art has put much effort into improving the computation time for statistical iterative reconstruction algorithms [4].

The class of maximum-likelihood expectation-maximization (MLEM) algorithms has been the leading statistical iterative reconstruction algorithms for several years [5]. Being applicable for Poisson Compton data in both the bin-mode [6] and list-mode [7], the conventional MLEM algorithm exhibits attractive properties including consistent and predictable convergence behavior, guaranteed non-negativity, and count preservation at each iteration. Nevertheless, since the algorithm is relatively slow, several variants have been proposed to speed up its convergence. The main improvements reside in using grids of different sizes to reduce processing time [8], extrapolating and increasing the magnitude of the change made at each iteration [9], updating each pixel individually with a series of different complete-data spaces [10], or in increasing the number of updates by using only part of the data in each update [11]. Despite their abundance, most MLEM algorithms only yield good reconstructed images when the parallax in the measurements is large enough. In other words, we cannot apply these algorithms to handheld Compton cameras that are becoming popular in nuclear engineering applications due to their convenience and economic advantages [12]. This fact prompted us to improve MLEM algorithms to address the lack of parallax inherent in handheld Compton cameras.

A solution is to measure potential radioactive sources with a handheld Compton camera deployed at different view angles, then combine the gathered data to increase the parallax [13]. Indeed, using *in turn* events recorded by an ultra-compact Compton camera from one view to another, Kishimoto *et al.* successfully locate radioactive sources in their experiments [14] with a conventional list-mode MLEM (LMMLEM) algorithm [7]. It is worth noting that the conventional LM-MLEM algorithm still works for single-view Compton data because the authors deployed the cameras very near to potential sources so that the parallax for each camera remains enough, albeit small. The major challenge in this current work is the *severe lack of parallax in single-view measurements*, which makes the existing LM-MLEM algorithms inapplicable. To overcome this challenge, we propose using multi-view Compton data

simultaneously to build a so-called *list-mode simultaneous data space* where each element is a set of independent events arbitrarily given from all the view angles. This new list-mode data leads to new probabilistic models for the system response matrix and sensitivity. Using the probability theory, we find that these models are the sum of all response matrices and sensitivity models of individual cameras deployed at different view angles. They are thus flexible and can inherit the state-of-the-art models previously proposed for single-view Compton data (see e.g., [15,16] and references therein). Following a similar formulation process as in [17], we arrive at an extended LM-MLEM algorithm adapted to the new list-mode simultaneous data. This extended version shares the same iteration equation form as in the conventional LM-MLEM algorithm, but with different meaning. To assess the performance of the proposed 3D reconstruction algorithm, we setup an experimental system with a punctual 0.2 (MBq) ^{22}Na source and a handheld CeBr3 Compton camera developed by Damavan Imaging [18] to obtain 1-view, 2-view and 3-view Compton data. Using an extension of the well-known Maxim *et al.*'s probabilistic model [19] as the basic camera response matrix and sensitivity, we apply the extended list-mode MLEM to determine the radioactive source location. Various numerical results with different numbers of views and different locations of the punctual source confirm the outperformances of our extended LM-MLEM 3D reconstruction algorithm.

We structure the remainder of the paper as follows. In Section II, we present the list-mode simultaneous data space, the associated model for the system response matrix and sensitivity, and an extended version of the conventional LM-MLEM algorithm under the assumption of the Poisson data model. We dedicate Section III to numerical experiments and analyses. Finally, we conclude the paper and give some perspectives for the future works in Section IV.

II. Extended LM-MLEM 3D Reconstruction Algorithm

Let consider a system consisting of a radioactive source located in an image volume $\boldsymbol{V}$ and a handheld Compton camera deployed at K different view angles around the volume $\boldsymbol{V}$ as in Fig. 1. Our goal is to reconstruct the radioactive source image from the multi-view Compton events measured by the camera.

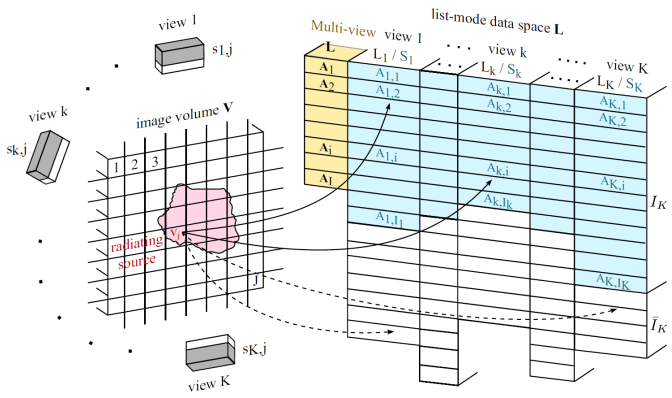

Fig. 1. Compton system, image volume and list-mode data-space.

A. List-Mode Data Space, Response Function and Sensitivity

Let divide the image volume $\boldsymbol{V}$ in to $J \in N^*$ voxels v_j, with $j \in \boldsymbol{\mathcal{J}} = \{1, \cdots, J\}$. A photon emitted from v_j and detected by the k-th view angle camera, with $k \in \boldsymbol{K} = \{1, \cdots, K\}$, is recorded as event $A_{k,i}$, $i = 1,2, \cdots$ of a list L_k. Each recorded event $A_{k,i}$ consists of 4 key attributes $\{P_{k,i,1}, E_{k,i,1}, P_{k,i,2}, E_{k,i,2}\}$ as illustrated in Fig. 2, where $P_{k,i,1}, P_{k,I,2} \in R^3$ are respectively the positions of the first and second interaction on the scatterer and absorber, and $E_{k,i,1}$ and $E_{k,i,2}$ are the associated energy. We

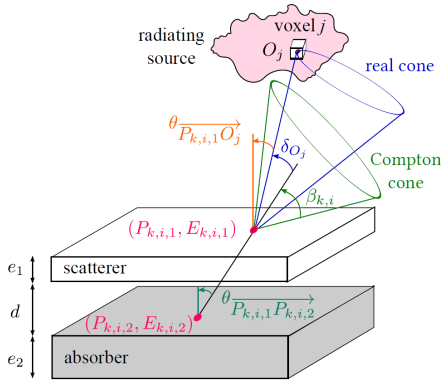

Fig. 2. Acquisition principle of the Compton camera at the k-th view angle.

call $A_{k,i}$ a valid event if $E_{k,i,1} + E_{k,i,2}$ satisfies a preset energy range. Among events recorded in list L_k, we assume I_k valid events constituting the unordered set $S_k \triangleq \{A_{k,1}, \cdots, A_{k,I_k}\}$. Each valid event generates a Compton cone, and the itersection of several resulting Compton cones can return an image of the radioactive source [20]. Unfortunately, the lack of parallax inherent in Compton cameras does not allow an efficient image reconstruction when using only events from a single view (i.e., it returns a direction toward the radioactive source rather than its location). That is why we should coordinate events from multi-views seeking parallax improvement and ultimately a better reconstruction result. Unlike Kishimoto *et al.* [14] who consider Compton event in turn from one view to another, we propose using events from all view angles simultaneously. It allows us to deal with the severe lack of parallax for which the 3D reconstruction from a certain view angle definitively fails. More precisely, we built a new list-mode data-space $\boldsymbol{L} = \{A_1, \ldots, A_i, \ldots, A_I\}$, where $I = \min\{I_1, \ldots I_k, \ldots, I_K\}$ denotes the length of $\boldsymbol{L}$ and $A_i \triangleq \cup_{k=1}^{K} A_{k,i}$, $i \in \mathcal{I} \triangleq \{1, \ldots, \mathrm{I}\}$, is a set of K independent valid events arbitrarily given from K view angles. We give in Fig .1 an illustration of the data list $\boldsymbol{L}$.

Using $\boldsymbol{L}$ for 3D reconstruction requires an associated system response matrix and sensitivity. Let denote t_{ij} an element of the *system* response matrix $\boldsymbol{T}$ indexed on the event A_i and on voxel v_j, it corresponds to the probability that photons emitted from v_j are detected by the system and recorded as A_i. Mathematically, we formulate t_{ij} as

$$t_{ij} = P(A_i, D|v_j) = P(A_i|D, v_j)s_j, \qquad (1)$$

where D stands for the event "*detected by the system*", and $s_j \triangleq P(D|v_j)$ is known as *system sensitivity*. Denoting D_k the event "*detected by the camera employed at the k-th view angle*", we

obtain $D = \cup_{k=1}^{K} D_k$ and further express t_{ij} by

$$t_{ij} = P\left(\cup_{k=1}^{K}\{A_{k,i}, D_k\}|v_j\right) = \sum_{k=1}^{K} t_{ijk}\,, \tag{2}$$

where $t_{ijk} \triangleq P\left(A_{k,i}, D_k|v_j\right)$ can be seen as an element of the camera response matrix $\boldsymbol{T}_k$ at the k-th view angle. Similarly, we obtain the system sensitivity s_j as

$$s_j = P\left(\cup_{k=1}^{K} D_k|v_j\right) = \sum_{k=1}^{K} s_{jk}\,, \tag{3}$$

where s_{jk} stands for the sensitivity of the k-th view angle camera. The sum over k in both the expressions (2) and (3) confirms that combining multi-view Compton events as in $\boldsymbol{L}$ can significantly improve the detection probability by the system, especially when a number of view angles becomes higher. It is worth noting that the expressions (2) and (3) constitutes a general framework for the system response and sensitivity. The models of camera response t_{ijk} and sensitivity s_{jk} have been extensively developed in the litterature. Despite their abundance, the camera response models share the same development method initially proposed by Wilderman *et al.* in [17]. Their differences reside mostly in the introduction of various kinds of measurement uncertainties (i.e., detector spatial resolution [19], detector energy resolution [21], Doppler broadening effect [22], etc.) to improve the model accuracy. Similarly, various models have been proposed for the camera sensitivity such as ones summarized by Muñoz *et al.* in [15].

B. eLM-MLEM Algorithm

We formulate here an extension of the conventional LM-MLEM algorithm for 3D reconstruction using the list-mode data space $\boldsymbol{L}$. For convenience, we first conduct the formulation under the bin-mode data as in [17], and then derive the model of interest by considering list-mode data as a limiting case of bin-mode when the bin widths tend to zero. This approach is motivated by the same information contained in the likelihood functions of both kinds of data albeit their different in format, so that the convergence properties of the corresponding LM-MLEM algorithms are identical [5]. By this way, we can define, for the bin-mode data, a vector of measurement $\boldsymbol{g}$ where each element g_i, $i \in \mathcal{I}$, is a random variable describing the number of counts in a virtual bin i corresponding the event A_i. When $g_i \to 1, \forall_i \in \mathcal{I}$, then the bin-mode data return to the list-mode ones [23]. Besides, we can also find in [7] a direct formulation for the list-mode data.

Let denote $\boldsymbol{f}$ the source distribution in the considered image volume $\boldsymbol{V}$, each element $f_j, \forall j \in \mathcal{J}$, of $\boldsymbol{f}$ characterizes the emission intensity of the voxel v_j in $\boldsymbol{V}$. Assuming the Poisson event-counting model [2], we obtain the conditional probability mass function of observing g_i given $\boldsymbol{f}$ as

$$p(g_i|\boldsymbol{f}) = e^{-\mu_i}\frac{\mu_i^{g_i}}{g_i!} \tag{4}$$

where $\mu_i = \sum_{j=1}^{J} t_{ij} f_j$ denotes the mean value of g_i. Reconstruct 3D image of a radioactive source is equivalent to find the estimate that maximizes the log-likelihood function $\mathcal{L}(\boldsymbol{g}|\boldsymbol{f})$

$$\hat{\boldsymbol{f}} = \arg\max_{\{\boldsymbol{f}\geq 0\}} \mathcal{L}(\boldsymbol{g}|\boldsymbol{f})\,, \tag{5}$$

where

$$\mathcal{L}(\boldsymbol{g}|\boldsymbol{f}) = \sum_{i=1}^{I}\left(-\sum_{j=1}^{J} t_{ij} f_j + g_i \ln\left(\sum_{j=1}^{J} t_{ij} f_j\right) - \ln(g_j!)\right). \tag{6}$$

By following the same procedure in [24] for the bin-mode data, we can characterize the E-step at the k-the iteration by the function

$$\mathcal{Q}_b\left(\boldsymbol{f}|\hat{\boldsymbol{f}}^{(k)}\right) = \sum_{i=1}^{I}\sum_{j=1}^{J}\left(\frac{g_i t_{ij}\hat{f}_j^{(k)}}{\sum_{s=1}^{J} t_{is}\hat{f}_s^{(k)}}\ln\left(t_{ij}f_j\right) - t_{ij}f_j\right), \tag{7}$$

where $\hat{\boldsymbol{f}}^{(k)}$ is the maximum likelihood estimate of $\boldsymbol{f}$ at the k-th iteration, and $\hat{f}_j^{(k)}$, $\forall j \in \mathcal{J}$, are elements of $\hat{\boldsymbol{f}}^{(k)}$. Approaching $g_i \to 1$, $\forall i \in \mathcal{I}$, we obtain the associated function for the list-mode data

$$\mathcal{Q}_l\left(\boldsymbol{f}|\hat{\boldsymbol{f}}^{(k)}\right) = \sum_{i=1}^{I}\sum_{j=1}^{J}\left(\frac{t_{ij}\hat{f}_j^{(k)}}{\sum_{s=1}^{J} t_{is}\hat{f}_s^{(k)}}\ln\left(t_{ij}f_j\right) - t_{ij}f_j\right). \tag{8}$$

In M-step, we maximize $\mathcal{Q}_l\left(\boldsymbol{f}|\hat{\boldsymbol{f}}^{(k)}\right)$ by merely vanishing its partial derivative with respect to f_j, $\forall j \in \mathcal{J}$, and obtain

$$f_j = \frac{\hat{f}_j^{(k)}}{\sum_i^I t_{ij}}\sum_{i=1}^{I}\frac{t_{ij}}{\sum_{s=1}^{J} t_{is}\hat{f}_s^{(k)}}. \tag{9}$$

Setting $s_{jk} \triangleq \sum_{i=1}^{I} t_{ijk}$, and using (2) and (3), we arrive to the estimate of $\boldsymbol{f}$ at the $(k+1)$-st iteration as

$$\hat{f}_j^{(k+1)} = \frac{\hat{f}_j^{(k)}}{s_j}\sum_{i=1}^{I}\frac{t_{ij}}{\sum_{s=1}^{J} t_{is}\hat{f}_s^{(k)}}, \quad \forall j \in \mathcal{J}, \tag{10}$$

where s_j is given by (3). Repeating (8) until verify a certain convergence criterion, we obtain the final maxim likelihood estimate $\hat{\boldsymbol{f}}$.

We can remark that the update equation (10) shares exactly the same form as the one of the conventional LM-MLEM algorithm. However, they do not have the same meaning. With t_{ij} and s_j defined by (2) and (3), ours takes into account simultaneously multi-view Compton events, and degenerates into the classical ones when only a single-view data are used. It is thus more generalized, flexible and can inherit the state-of-the-art models previously proposed for t_{ijk} and s_{jk}. We call therefore the proposed algorithm extended LM-MLEM (eLM-MLEM).

III. Numerical Experiments and Analyses

We present in this section an experimental system that can generate various configurations of real multi-view Compton data in function of the view number, the source location and the energy range. These rich data allow assessing thoroughly the performance of the proposed eLM-MLEM 3D reconstruction algorithm.

A. Experiments Setting and Data

To obtain real data for performance assessment, we setup an experimental system consisting of a punctual 0.2 (MBq) ^{22}Na source and a handheld CeBr3 Compton camera developed by Damavan Imaging [18]. We deploy sequentially the camera at

three different view-angles as in Fig. 3: *the two first views are set perpendicularly on a same horizontal plane* ***H*** *of the punctual source, while the third view is placed vertically above.*

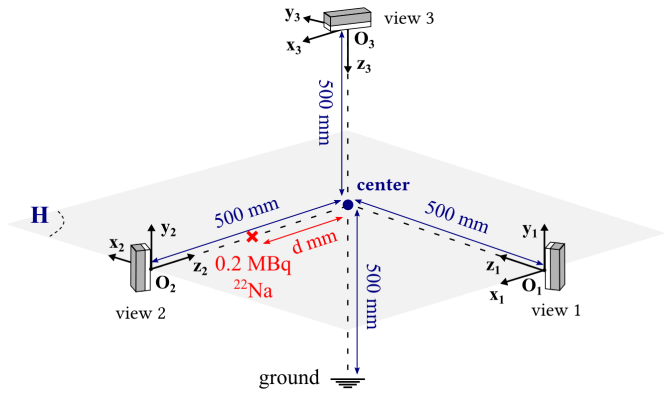

Fig. 3. Experiment setting with one punctual source and three view-angles.

The distance between the camera and the center is 500 (mm), and all the system is located 500 (mm) from the ground. We locate the punctual 0.2 (MBq) ^{22}Na source on the plane **H** at d (mm) from the center. For each location of the radioactive source, we conducted the data acquisition within 15 minutes per view-angle. Table I shows the number of Compton events recorded from three view-angles for different energy ranges depicted in Fig. 4. The events satisfying the low energy range

TABLE I
NUMBER OF COMPTON EVENTS IN FUNCTION OF SOURCE LOCATION, ENERGY RANGE AND VIEW ANGLE

d (mm)	Energy range (MeV)	Number of Compton events / view		
		view 1	view 2	view 3
0	full range	1339	1398	1308
	[1.15, 1.38]	140	148	140
	[0.48, 0.54]	344	335	335
250	full range	1951	5132	987
	[1.15, 1.38]	96	279	56
	[0.48, 0.54]	288	541	104

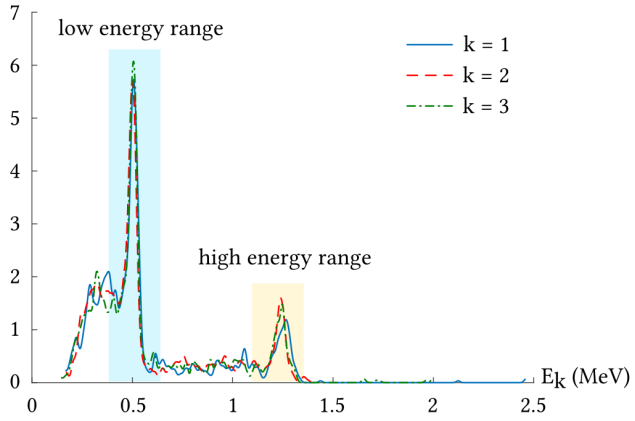

Fig. 4. Spectra of energies.

[0.48, 0.54] and the high energy range [1.15, 1.38] are selected to constitute different 1-view, 2-view and 3-view datasets.

B. Experimental Results and Analyses

The eLM-MLEM 3D reconstruction algortihm requires a probabilistic model for the camera response t_{ijk} and sensitivity s_{jk}. Among various choices (see Subsection II.A), we adopt the model t_{ijk} proposed by Maxim *et al.* in [19] and add different measurement uncertainties related to the spatial and energy resolution of detectors, as well as the Doppler broadening effect to make the model more flexible. This extended model leads us to set the camera sensitivity as uniform $s_{jk} = 1$ because uncertainties have been taken into account in t_{ijk}.

Using 3-view datasets at high range energy, we show in Fig. 5 and Fig. 6 how the reconstructed 3D image evolves in function of iteration number for two locations of the radioactive souces $d = 0$ and $d = 250$ (mm). The eLM-MLEM algorithm

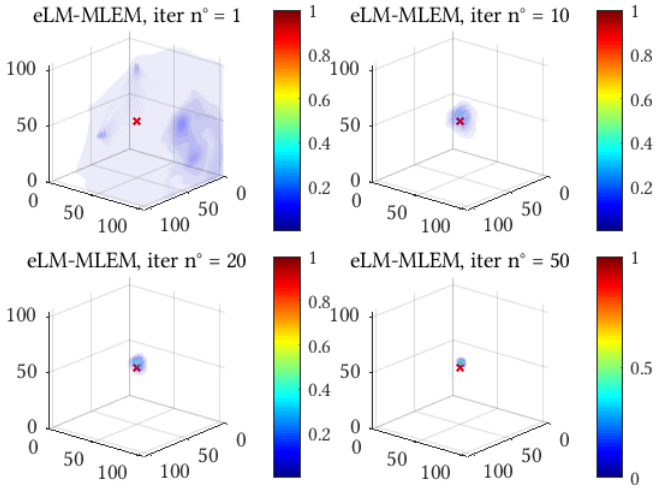

Fig. 5. Convergence of the eLM-MLEM algorithm when $d = 0$ (mm).

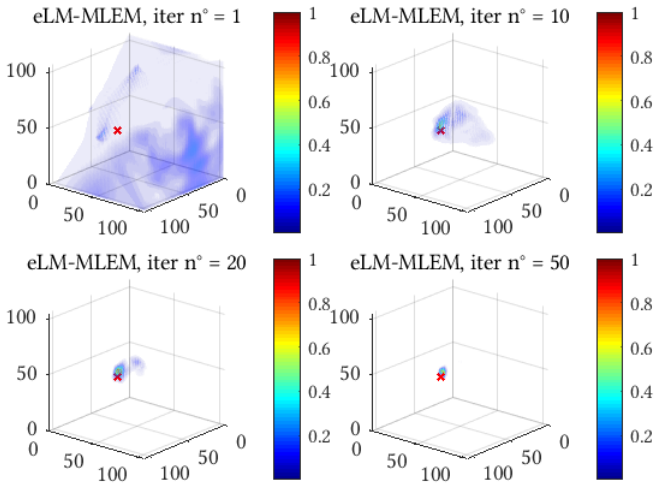

Fig. 6. Convergence of the eLM-MLEM algorithm when $d = 250$ (mm).

converges since 50th iteration. Consider now the datasets at high range energy of the radioactive source $d = 0$ (mm), we give in Fig. 7 the recontructed results given by the well-kown back-projection and the eLM-MLEM algorithm, as well as the X-Y, Y-Z and X-Z profiles for different multi-view datasets. When the 1-view data are used, the eLM-MLEM algorithm returns to

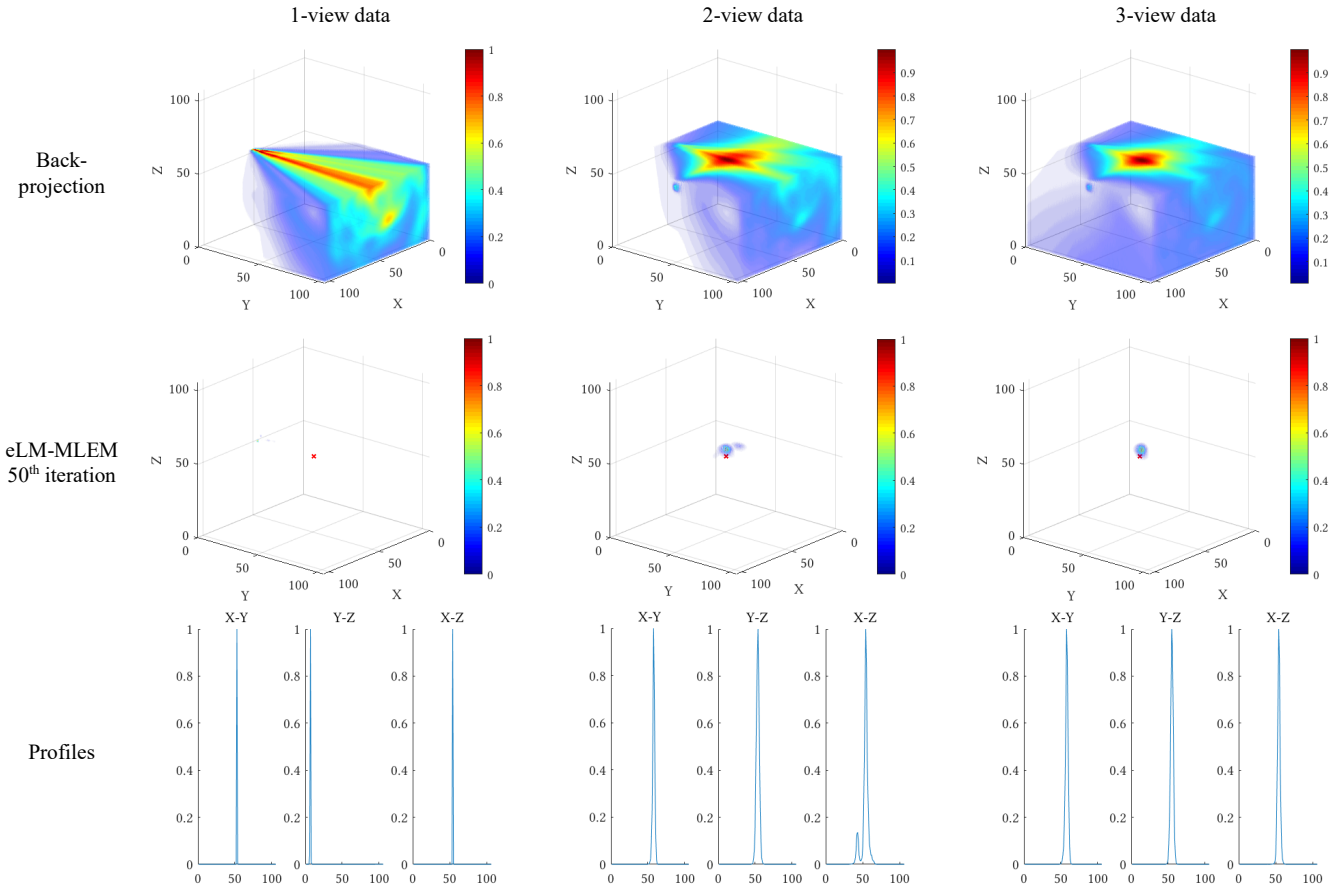

Fig. 7. Recontructed results given by the well-kown back-projection and the eLM-MLEM algorithm, as well as the X-Y, Y-Z and X-Z profiles.

the conventional LM-MLEM algorithm. Clearly, the reconstruction fails in the case of 1-view data and succeeds in the cases of 2-view and 3-view data. This confirms the outperformance of the eLM-MLEM algorithm over the conventional one. Looking at the reconstructed image at the 50th iteration and their profiles, we find that the higher number of views allow a better result.

For a quantitative assessement, we propose using the so-called *sum of weighted distances* (SWD) between the reconstructed point cloud and the true source as a criterion for the quality assessment at the k-th iteration

$$SWD^{(k)} = \sum_{j=1}^{J} \hat{f}_j^{(k)} \left\| P_j - P_S \right\|_2,$$

where $\hat{f}_j^{(k)}$ is given from (10), P_j and P_S are respectively the coordinate vectors of the voxel v_j and the punctual source, and $\|\cdot\|_2$ denotes the Euclidean norm. The lower the value of $SWD^{(k)}$, the more the reconstructed 3D image is near to the true source. We show in Table II the $SWD^{(k)}$ scores when the 2-view and 3-view data at the low and high energy range are used to reconstruct both the radioactive sources $d = 0$ and $d = 250$ (mm). The lower scores obtained by the 3-view data justify the relevance in using higher number of view-angles for the 3D image reconstruction.

TABLE II
SUM OF WEIGHTED DISTANCES BETWEEN THE RECONSTRUCTED POINT CLOUD AND THE TRUE SOURCE LOCATION

Data	Low energy range		High energy range	
	$d = 0$	$d = 250$	$d = 0$	$d = 250$
2-view	6943.2	9199.2	7846.9	3588.4
3-view	5271.2	4728.5	4046.9	1587.7

IV. CONCLUSIONS AND PERSPECTIVES

We have developed in this work an extended LM-MLEM 3D reconstruction algorithm adapted to multi-view Compton data. Based to real multi-view data of punctial radioactive source, we prove that the algorithm is effective for the serious lack of parallax in measurements. Especially, the higher the number of view-angles in the Compton data, the more the algorithm return better results.

Albeit very promising results, we can remark that the algorithm still converges slowly. A way to speed up it is to apply the variants of the conventional LM-MLEM algorithm introduced in Section I to the eLM-MLEM algorithm. However, such a solution always requires a large number of Compton events for noise reduction. To overcome this problem, we think about a 3D reconstruction algorithm in the Bayesian framework with a prior reflecting the smoothness in the expected image. It is the main orientation of our future works.

ACKNOWLEDGMENT

This research was financially supported by ANR RED-7D project and BPI PIA4 DreamScanner project.

REFERENCES

[1] P. E. Kinahan, M. Defrise and R. Clackdoyle, "Analytic image reconstruction methods", in *Emission Tomography: The Fundamentals of PET and SPECT*, Elsevier Academic Press, 2004, pp. 421-442.

[2] D. S. Lalush and M. N. Wernick, "Iterative image reconstruction", in *Emission Tomography: The Fundamentals of PET and SPECT*, Elsevier Academic Press, 2004, pp. 443-472.

[3] V. Maxim, "Filtered backprojection reconstruction and redundancy in Compton camera imaging", *IEEE Transactions on Image Processing*, vol. 23, no. 1, 2014, pp. 332-341.

[4] B. F. Hutton, "Recent advances in iterative reconstruction for clinical SPECT/PET and CT", *Acta Oncologica*, vol. 50, no. 6, 2011, pp. 851-858.

[5] J. Qi and R. M. Leahy, "Iterative reconstruction techniques in emission computed tomography", *Physics in Medicine & Biology*, vol. 51, no. 15, 2006, pp. R541.

[6] L. A. Shepp and Y. Vardi, "Maximum Likelihood Reconstruction for Emission Tomography", *IEEE Transactions on Medical Imaging*, vol. 1, no. 2, 1982, pp. 113-122.

[7] L. Parra and H. H. Barrett, "List-Mode Likelihood: EM Algorithm and Image Quality Estimation Demonstrated on 2-D PET", *IEEE Transactions on Medical Imaging*, vol. 17, no. 2, 1998, pp. 228-235.

[8] M. V. Ranganath, A. P. Dhawan and N. Mullani, "A multigrid expectation maximization reconstruction algorithm for positron emission tomography", *IEEE Transactions on Medical Imaging*, vol. 7, no. 4, 1988, pp. 273-278.

[9] L. Kaufman, "Implementing and accelerating the EM algorithm for positron emission tomography", *IEEE Transactions on Medical Imaging*, vol. 6, no. 1, 1987, pp. 37-51.

[10] J. Fessler and A. O. Hero, "Space-alternating generalized expectation-maximization algorithm", *IEEE Transactions on Signal Processing*, vol. 42, no. 10, 1994, pp. 2664-2677.

[11] H. M. Hudson and R. S. Larkin, "Accelerated image reconstruction using ordered subsets of projection data", *IEEE Transactions on Medical Imaging*, vol. 13, no. 4, 1994, pp. 601-609.

[12] Y. Sato, Y. Terasaka, W. Utsugi, H. Kikuchi, H. Kiyooka and T. Torii, "Radiation imaging using a compact Compton camera mounted on a crawler robot inside reactor buildings of Fukushima Daiichi Nuclear Power Station", *Journal of Nuclear Science and Technology*, vol. 56, no. 9-10, 2019, pp. 801-808.

[13] A. Kishimoto, J. Kataoka, T. Nishiyama, T. Taya and S. Kabuki, "Demonstration of three-dimensional imaging based on handheld Compton camera", *Journal of Instrumentation*, vol. 10, no. 11, 2015, pp. P11001.

[14] A. Kishimoto, J. Kataoka, T. Taya, L. Tagawa, S. Mochizuki, S. Ohsuka, T. Nagao, K. Kurita, M. Yamaguchi, N. Kawachi, K. Matsunaga, H. Ikeda, E. Shimosegawa and J. Hatazawa, "First demonstration of multi-color 3-D in vivo imaging using ultra-compact Compton camera", *Scientific reports*, vol. 7, no. 1, 2017, pp. 2110.

[15] E. Muñoz, J. Barrio, J. Bernabéu, A. Etxebeste, C. Lacasta, G. Llosá, A. Ros, J. Roser and J. F. Oliver, "Study and comparison of different sensitivity models for a two-plane Compton camera", *Physics in Medicine & Biology*, vol. 63, no. 13, 2018, pp. 135004.

[16] C. Wu, S. Zhang and L. Li, "An accurate probabilistic model with detector resolution and Doppler broadening correction in list-mode MLEM reconstruction for Compton camera", *Physics in Medicine & Biology*, vol. 67, no. 12, 2022, pp. 125017.

[17] S. J. Wilderman, N. H. Clinthorne, J. A., Fessler and W. L. Rogers, "List-mode maximum likelihood reconstruction of Compton scatter camera images in nuclear medicine", in *IEEE Nuclear Science Symposium Conference Record*, vol. 3, 1998, pp. 1716-1720.

[18] M. Z. Hmissi, A. Iltis, C. Tata, G. Zeufack, L. Rodrigues, B. Mehadji, C. Morel and H. Snoussi, "First images from a CeBr 3/LYSO: Ce Temporal Imaging portable Compton camera at 1.3 MeV", in *2018 IEEE Nuclear Science Symposium and Medical Imaging Conference Proceedings*, Sydney, NSW, Australia 2018, pp. 1-3.

[19] V. Maxim, X. Lojacono, E. Hilaire, J. Krimmer, E. Testa, D. Dauvergne, I. Magnin and R. Prost, "Probabilistic models and numerical calculation of system matrix and sensitivity in list-mode MLEM 3D reconstruction of Compton camera images", *Physics in Medicine & Biology*, vol. 61, no. 1, 2016, pp. 243.

[20] L. C. Parra, "Reconstruction of cone-beam projections from Compton scattered data", *IEEE Transactions on Nuclear Science*, vol. 47, no. 4, 2000, pp. 1543-1550.

[21] B. Mehadji, M. Dupont, Y. Boursier and C. Morel, "Extension of the List-Mode MLEM Algorithm for Poly-Energetic Imaging with a Compton Camera", in *2018 IEEE Nuclear Science Symposium and Medical Imaging Conference*, 2018, pp. 1-8.

[22] Y. Feng, J. M. Létang, D. Sarrut and V. Maxim, "Influence of Doppler broadening model accuracy in Compton camera list-mode MLEM reconstruction", *Inverse Problems in Science and Engineering*, vol. 29, no. 13, 2021, pp. 3509-3529.

[23] H. H. Barrett, T. White and L. C. Parra, "List-mode likelihood", *Journal of the Optical Society of America A*, vol. 14, no. 11, 1997, pp. 2914-2923.

[24] K. Lange and R. Carson, "EM Reconstruction Algorithms for Emission and Transmission Tomography", *Journal of Computer Assisted Tomography*, vol. 8, no. 2, 1984, pp. 306-316.